The formation of gradients in wet deposited coatings with photocatalytically active nanoparticles

H. SCHMIDT *, M. AKARSU, TH. S. MÜLLER, K. MOH, G. SCHÄFER, D. J. STRAUSS and M. NAUMANN

Leibniz-Institut für Neue Materialien, Im Stadtwald, Geb. 43 A, 66123 Saarbrücken, Germany

Abstract—A total of 81 doped and undoped anatase nano-particles were synthesised by a precipitation/co-precipitation process followed by a hydrothermal treatment to obtain increased visible light photocatalytic activity. The screening process was performed utilising a high throughput analysis system based on the photometric monitoring of the photocatalytic degradation of organic dyes (Rhodamine B, Malachite Green, Acid Blue 29). Photocatalytically active coatings were prepared with selected catalysts with high and low rankings from the screening. Degradation experiments with stearic acid could confirm the varying grades of visible light activity as seen in the screening process.

Keywords: Nanoparticle; photocatalysis; anatase; dye degradation; coating.

INTRODUCTION

The development of highly efficient photocatalysts has become of increased importance since the high potential of photocatalytically active surfaces, for example, self-cleaning and self-sterilizing properties, has been shown for many industrial applications. After the development of the field by Fujishima [1, 2] and Hashimoto [2, 3] and the first applications shown by TOTO [4–6], the field exploded considerably. The photocatalytic effect of TiO_2 as a photo semiconductor is not new as, for example, shown by Hermann. This effect is depending on the lattice defects of TiO_2 and can be quenched considerably by lattice doping [7]. Due to the band gap energy of about 3.2 eV, the light absorption of TiO_2 especially anatase takes place in the UV. For this reason, much research is going on at present in order to develop so-called visible lights photocatalysts because there is much more energy produced by the sunlight in the visible lights regime compared to the UV. First positive results have been already demonstrated by Kisch [8–10] with carbon-doped photocatalysts

*To whom correspondence should be addressed. E-mail: schmidt@inm-gmbh.de

[11] and by Taga from Toyota with nitrogen-doped catalysts [12]. Sn-doped titania also shows enhanced day-light activity [13].

Due to the large number of possible variations it is rather difficult to find out the appropriate compositions and concentrations of dopants, especially if lattice doping should be avoided. For these reasons, investigations have been carried out to find out how far a combinatorial pre-screening may help to accelerate the development of efficient daylight catalysts, and a dye decolouration screening technology with high throughput has been developed.

EXPERIMENTAL

General photocatalyst preparation

334.912 g $Ti(OiPr)_4$ was mixed with 73.84 g 1-propanol at room temperature. After 5 min stirring a mixture of 5.124 g 37 wt% HCl and 40 g 1-propanol was added and stirred for another 10 min followed by addition of a mixture of 6.124 g water and 60 g 1-propanol with intensive stirring during 10 min and stirred for 10 more min.

127.5 g of the derived sol (containing 14.2 wt% $Ti(OiPr)_4$) was transferred into a 250-ml Teflon® crucible, and the required amount of dopant precursor was added. Homogenization was archived after ultrasonic treatment. The mixture was then left in a preheated (225°C) stainless steel autoclave device and in general held at 225°C for 90 min. The doping and treatment conditions are given in Tables 1–3.

Dry, redispersable nanopowders of photocatalysts were obtained after removal of solvents by vacuum distillation. These catalyst materials were used for the described screening process.

For the batches with higher $Ti(OiPr)_4$ concentrations (samples 64, 65, 66, 69, 71 and 72) the above stated procedure for obtaining the titania sol was modified by increasing the amount of $Ti(OiPr)_4$ and adjusting the amounts of water and HCl, while keeping the amounts of propanole and the procedure constant. Further photocatalyst preparation details are given in Ref. [14].

High-throughput screening of photocatalyst nanopowders

The dry photocatalyst (5 wt% photocatalyst) nanoparticles were re-dispersed in 1 wt% HCl by ultrasonic treatment followed by stirring and the catalyst suspensions transferred to 96-well PS multititer-plates (MTP) with an automated liquid handling system (Tecan Genesis RSP 150). A schematic depiction of the high throughput equipment is shown in Fig. 1. In detail, each catalyst sample was divided in 2×12 portions of 50 μl per cavity and mixed with 150 μl aqueous dye solutions (6 ppm Rhodamine B, 3 ppm Malachite Green, 180 ppm Acid Blue 29) or 150 μl water for the background measurements. The plates were sealed with a PS cap, left for 1 h in the dark and $t = 0$ min vis spectra were aquired with a MTP-reader (Molecular Devices Spectramax 190, $\lambda = 400$–800 nm, $\Delta\lambda = 2$ nm). Afterwards, samples

Table 1.
Doped TiO_2 catalysts

Sample	Precursor	Concentration (mol%)	Sample	Precursor	Concentration (mol%)
2	$VO(acac)_2$	0.5	32	$MoCl_4$	0.25
3		1	33		0.5
4		2.5	34		1
5		5	35		2.5
6	$Cr(NO_3)_3$	0.5	36	$In(OAc)_3$	0.5
7		1	37		1
8		5	38		5
9	$Mn(NO_3)_3$	0.5	39		7.5
10		1	40	$SnCl_4$	0.5
11		5	41		1.25
12	$Fe(NO_3)_3$	0.5	42		5
13		1	43		7.5
14		5	44	$Ce(NO_3)_3$	0.5
15		10	45		1
16	$Co(OAc)_2$	0.5	46		5
17		1	47		7.5
18		5	48	$Ce(OMeOEt)_4$	0.5
19		10	49		1
20	$CuCl_2$	0.5	50		2.5
21		1	51		5
22		5	52	$(NH_4)_2Ce(NO_3)_6$	0.5
23		10	53		1
24	$Cu(OEt)_2$	0.5	54		2.5
25		1	55		5
26		5	56	$Nd(OMeOEt)_3$	0.5
27		10	57		1
28	$Zn(acac)_2$	1	58		2.5
29		2.5	59		5
30		5	60	WCl_6	0.5
31		10	61		1
			62		5
			63		10

General preparation conditions: 14.2 wt% $Ti(OiPr)_4$, 225 °C, 90 min.

Table 2.
Undoped TiO_2 catalysts

Sample	$Ti(OiPr)_4$ (wt%)	T (°C)	t (min)
1	14.2	225	90
64	35.0	200	60
65	35.0	250	60
66	35.0	225	60

Table 3.
$SnCl_4$-doped TiO_2 catalysts

Sample	$SnCl_4$ (mol%)	$Ti(OiPr)_4$ (mol%)	T (°C)	t (min)
40	0.5	14.2	225	90
41	1.25	14.2	225	90
42	5	14.2	225	90
43	7.5	14.2	225	90
67	0.5	14.2	250	120
68	1	14.2	250	120
69	1	35.0	225	90
70	2.5	14.2	250	120
71	5	35.0	225	90
72	5	20.0	225	90

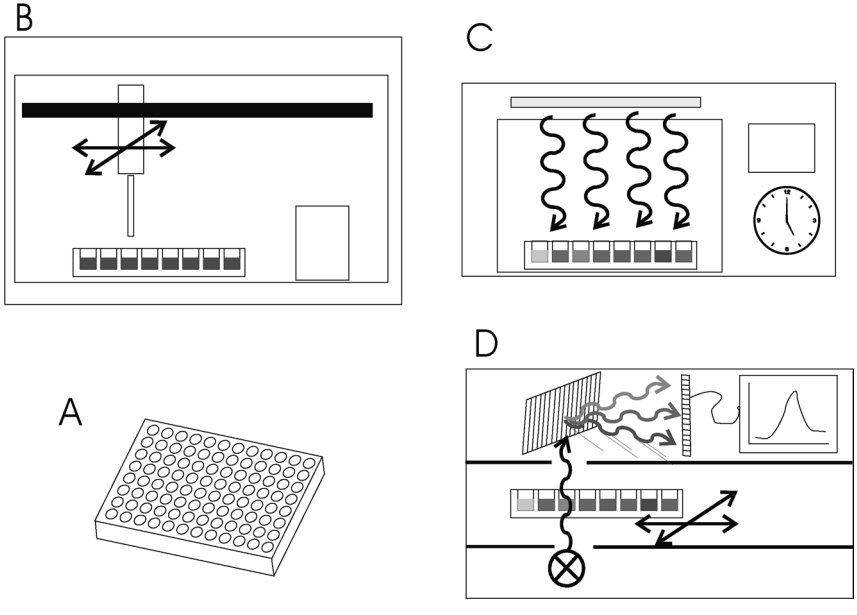

Figure 1. Schematics of the high-throughput testing equipment. (A) 96-well PS multititer plates (MTP); (B) pipetting robot and automated liquid handling system (Tecan Genesis RSP 150); (C) illumination with a suntester solar simulator Atlas-Suntest CPS+, 750 W/m^2 Xenon lamp; (D) UV-Vis spectrometer for 96-well plate with grating monochromator and CCD-line detector (Molecular Devices Spectramax 190, $\lambda = 400$–800 nm, $\Delta\lambda = 2$ nm).

were irradiated with a sun tester (Atlas-Suntest CPS+, 750 W/m^2 Xenon lamp) for 5 min (without cut-off filter), or 20 min (with 400 nm cut-off filter) without shaking, followed by a second acquisition of vis-spectra. The raw data was averaged three samples per dye-catalyst-irradiation-type and the background data substracted. Then, individual spectra of irradiated samples were integrated (Rhodamine B 450–620 nm, Malachite Green 535–700 nm, Acid Blue 29 450–700 nm) and divided

Table 4.
Semiconductor nanoparticle-doped catalysts (general preparation conditions: 14.2 wt% $Ti(OiPr)_4$, 225 °C, 90 min)

Sample	Particle type	Concentration (wt%)
73	WO_3	0.5
74		1
75		2.5
76		5
77		7.5
78	ITO	1
79		2.5
80		5
81		7.5

by similarly treated data of $t = 0$ min spectra. Thus, the obtained values are dimensionless.

For the subsequent ranking, the data was normalized with respect to the degree of photodegradation (DOP) of the different catalysts on the individual dyes. Based on the normalized data, the catalysts were arranged in decreasing order using the averaged minimum of the DOP. The lower the DOP, the better the performance (data not shown).

The variation of the doping and treatment conditions is listed in Tables 1–4. Doping was carried out with transition-metal ions, main group metal ions and rare earth metal ions, respectively. The dopants were selected with regard to low toxicity, high solubility in the alcoholic solvent and easy commercial availability.

The dopant concentrations (mol per mol Ti-precursor) were varied between 0.5 and 10 mol%. Samples 1 and 64–66 represent undoped anatase treated under different conditions.

The biggest group of dopants are transition metals. Samples 2–5 represent vanadium doped obtained from vanadium(II)acetylacetonate. Samples 6–8 represent chromium(II)nitrate-doped samples. Samples 9–11 are doped with manganese(II)nitrate. Samples 12–15 correspond to iron(III)nitrate-doped samples and samples 16–19 denote cobalt(II)acetate-doped material.

Copper-doped samples obtained from copper(II)chloride are listed as samples 20–23 and from copper(II)ethylate as samples 24–27. Samples 28–31 represent zinc-acetylacetonate-doped samples. Samples 32–35 stand for materials doped with molybdenum(IV)chloride and the samples 60–63 correspond to tungsten(VI) chloride-doped catalysts.

The rare metals are represented by Ce and Nd. Samples 44–47 are doped with cerium(III)nitrate, 48–51 represent samples doped with $Ce(OMeOEt)_4$, 52–55 are corresponding to samples doped with the cerium(IV)hexanitrato ammonium complex and 56–59 represent $Nd(OMeOEt)_3$-doped material.

Furthermore, In was chosen and is represented in the samples with the numbers 36–39. Samples 40–43 and 67–72 are corresponding to tin(VI)chloride-doped materials.

Furthermore, also oxidic semiconductor nanoparticles were added to the above-mentioned titania sol with the idea to form seeds on which the anatase phase is growing. Samples 73–77 represent WO_3 and 78–81 indium-tin-oxide (ITO), respectively.

Surface modification of the selected powders

2 g of the selected photocatalytically active powder was suspended in 20 ml dry toluene and treated for 15 min in an ultrasonic bath. 2.5 g hexadecyl trimethoxysilane was slowly added to this sol over 15 min. The sol was kept in the dark and stirred over night. Afterwards it was refluxed for 1 h (bath temperature 130°C). The solvent was removed by a rotary evaporator at reduced pressure (40°C bath temperature, end pressure < 1000 Pa). For the application, sols of 2% modified particles in heptane were prepared.

Binder system

36.6 g methyltriethoxysilane, 11.59 g tetraethoxysilane and 20.4 g Levasil 300/30 (an aqueous silica sol by Bayer) were mixed and stirred vigorously. 0.43 g 32% HCl was quickly added in one step. The reaction is exothermal and the mixture is stirred for 30 min until the sol is cooled down to ambient temperature. The mixture is diluted by the addition of 144 g isopropanol. The mixture has to be filtrated using a 0.8 μm filtration membrane.

Preparation of photocatalytically active double layer coatings

The application of the coatings was done on glass plates (10 by 10 cm) by dip-coating. In a first step the binder system was applied at a drawing speed of 2.5 mm/s. The wet film was allowed to pre-dry at room temperature, followed by a 1 h heat treatment at 80°C.

In the second step the active material was applied at a drawing speed of 4.5 mm/s from a 2 wt% sol of the surface-modified particles in heptane. The wet film was dried at room temperature, and then the coated plates were transferred into an oven. The temperature was brought to 450°C at a rate of 2°C/min and kept at 450°C for 1 h. The cooling down took place in the closed oven.

Preparation of photocatalytically active single layer coatings

1 g dry titania particles was stirred in 9 g dry toluene and a solution of 0.268 g stearic acid in 5 g dry toluene was added. By ultrasonic agitation for at least 15 min a sol was obtained. The sol was mixed with 0.146 g 3,3,4,4,5,5,6,6,7,7,8,8,8-tridecafluorooctyl-1,1,1-triethoxysilane (FTS) and stirred in the dark for 16 h.

Afterwards the solvents were evaporated using a rotary evaporator at 40°C bath temperature and reduced pressure to obtain a dry powder. Further drying can be executed in an evacuated drying chamber over night at 40°C.

150 mg of the FTS-modified particles were dispersed in 10 g dry 2-butanone (ethyl methyl ketone, MEK) by ultrasonic agitation. This was mixed with 50 g of the binder-system as described above and treated in an ultrasonic bath to obtain a clear sol for coating.

The application of the coatings was done on glass by dip-coating at a speed of 4.5 mm/s of the wet film was allowed to pre-dry at ambient temperatures before the coated substrates were transferred into an oven. They were heated to 450°C at a rate of 2°C/min and kept there for 1 h.

Stearic acid degradation experiments

For the stearic acid degradation experiments 5 by 5 cm pieces of the above-mentioned photocatalytically-coated glass plates were over coated by a layer of stearic acid by dip-coating. The solution of the stearic acid in heptane was hot saturated and had a concentration of 1.2 wt% stearic acid after cooling down to room temperature. The films were drawn 10 times at a speed of 8.5 mm/s. For comparison also uncoated glass plates were coated by the same technique, in order to correct for influences of effects such as evaporation or photolysis of the stearic acid.

The irradiation was executed using different light sources:

1. A Suntester type Suntest CPS by Heraeus/Atlas (Xenon Lampe, 1100 W, and irradiated area about 560 cm^2) in which next to the standard IR-heat protection filter a filter made by UV-transmissive special glass was installed (Fig. 7).
2. In this sun tester a second set of samples was irradiated through a filter foil with an edge at 400 nm cutting off the UV-radiation (Fig. 8).

The degradation of the stearic acid was followed by determination of the contact angle of the surface against water. The determination was executed by a computer-based video analysis system (Krüss G2/G40).

RESULTS AND DISCUSSION

Particle synthesis and characterization

We will only discuss some major aspects of the preparation and the characterization of the particles. More details can be found elsewhere [15].

The titania samples were prepared with a three-step process. First an amorphous undoped titania nano-particle sol was prepared by an acid-catalyzed precipitation process which was followed by the addition of the selected dopant. Finally a lyothermal treatment of the sols leads to the formation of anatase from the titania sol.

For all dopants concentration of 1 mol% and/or 5 mol% could be synthesised. In some cases the attempts to synthesise particles with 10 mol% were not successful, these attempts are not included in the lists (Tables 1–4).

The photocatalyst samples from the batches (1–72) consist of agglomerate-free nano-particles with an average size of 4–10 nm, as determined by HR-TEM measurements. XRD data show the dominance of anatase signals for most of the samples with only slight variations of the lattices parameters contributed to the influences of the dopant. A few exceptions where by-products (CuCl was found in samples 22 and 23) or mainly amorphous products (sample 51) have also been detected.

The dry powder samples can be easily dispersed in aqueous HCl (pH about 2), forming transparent or only slightly translucent sols with solid contents of 5% or more. This is indicating that the obtained powders are agglomerate free.

High-throughput screening

In order to estimate the efficiency, dye decolourisation was chosen since it is a very hopeful tool for high throughput methods. One has taken into consideration that this decolourisation may have different reasons which only partly were related to photocatalysis. In order to avoid incorrect interpretations, for example, caused

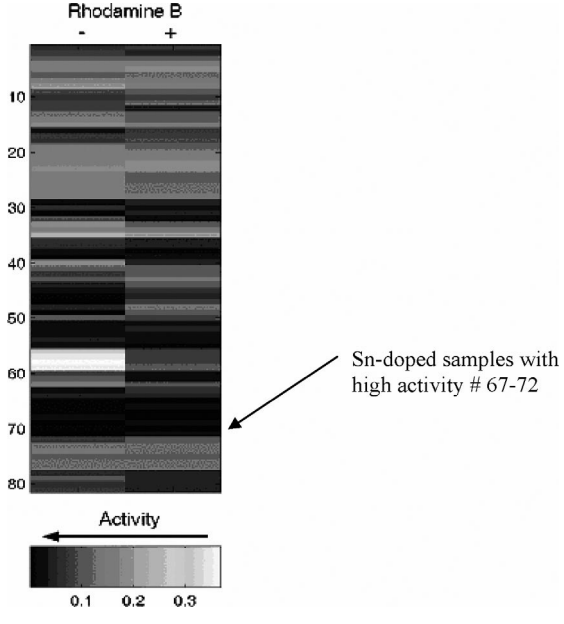

Figure 2. Result of the high-throughput screening experiments during degradation of Rhodamine B: depicted are two bands of colour-coded stripes representing the DOP values for the 81 different samples (top–down, see Tables 1–4 for the different dopants) for the activity of the respective catalysts for 5 min full spectrum irradiation (left column, −) or 20 min irradiation through a 400 nm cut-off filter (right column, +). Lower DOP values represent higher activity and are shown in darker colours.

by photosensitisation in the decomposition process, three different types of dyes have been tested which all have different electronic properties. The investigated dyes were Rhodamine B (a xanthene-type dye, concentration 6 ppm), Malachite Green (a triphenyl-methane-type dye, 3 ppm) and Acid Blue 29 (an azo-type dye, 180 ppm). The concentrations of the corresponding stock solutions had been optimized for the photometric measurement with a 96-well UV-Vis plate reader.

In the following, the results of the high-throughput screening with 81 variation parameters as already described in Section 2 are shown in Figs 2–4. Dark colours indicate high and bright colours low activity. For each dye tested two bands of colour-coded stripes for the 81 different samples (top to down, see Tables 1–4 for the different dopants) are displayed. The activity of the respective catalysts for 5 min full spectrum irradiation (left-hand column, −) or 20 min irradiation through a 400 nm cut-off filter (right-hand column, +) are colour coded and expressed as degree of photo degradation (DOP). Higher activity, which corresponds to lower DOP values, is shown in darker colours. It is important to recognise that these activity scales are not the same for the different dyes!

The spectra for the full scale irradiation and the irradiation through the cut-off filter are shown in Fig. 5. It can clearly be seen where the cut-off filter kicks in.

From the depicted results one can easily see that the degradation behaviour of the different dyes is varying for the various catalyst samples. Thus also the obtained

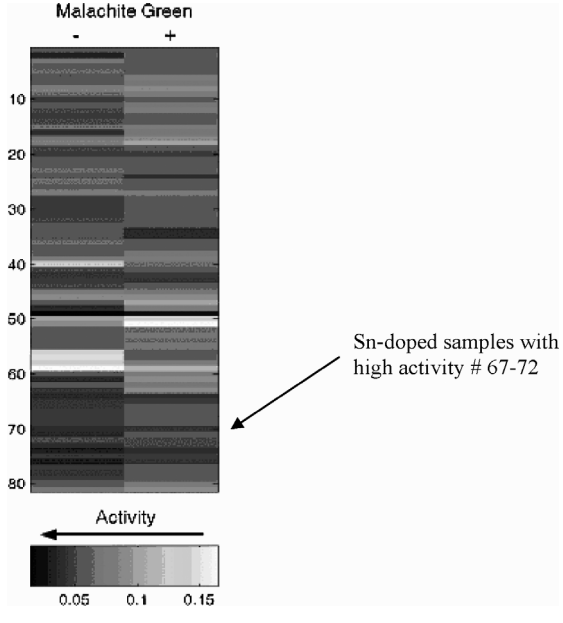

Figure 3. Result of the high-throughput screening experiments during degradation of Malachite Green: depicted are two bands of colour-coded stripes representing the DOP values for the 81 different samples (top–down, see Tables 1–4 for the different dopants) for the activity of the respective catalysts for 5 min full spectrum irradiation (left column, −) or 20 min irradiation through a 400 nm cut-off filter (right column, +). Lower DOP values represent higher activity and are shown in darker colours.

GOP values for the three different dyes under the different illumination conditions varied.

For Rhodamine B, the DOP values obtained under the experimental conditions are in the range of 0.0051 to 0.3675. Here a significant number of catalysts had high activities with DOP < 0.01. For the full spectrum illumination these were samples 47, 39, 69, 71, 31, 70, 46, 49, 65, representing samples doped by Ce, Sn, In and Zn, as well as an undoped sample (65). For the visible spectrum only irradiation experiment samples 70, 67, 68, 65, 55 were samples doped with Sn with the three best results followed by an undoped sample (65) and finally a Ce-doped catalyst.

For Malachite Green, the DOP values obtained under the experimental conditions are in the range of 0.0116 to 0.8583. Here a number of catalysts had high activities with DOP < 0.045. For the full spectrum illumination these samples were no. 75, 42, 57 and 70, representing samples doped by W, Sn and Nd. For the visible spectrum only irradiation experiment the sample no. 15, 14, 70 and 43 were samples doped with Fe and Sn.

For Acid Blue 29, the scale of the DOP values varied from 0.014 to 0.165. Here is only one catalyst with sample no. 49 which is doped by Ce, which shows good activity in both full spectrum with a DOP of 0,01408 and the visible with a DOP of 0,02459.

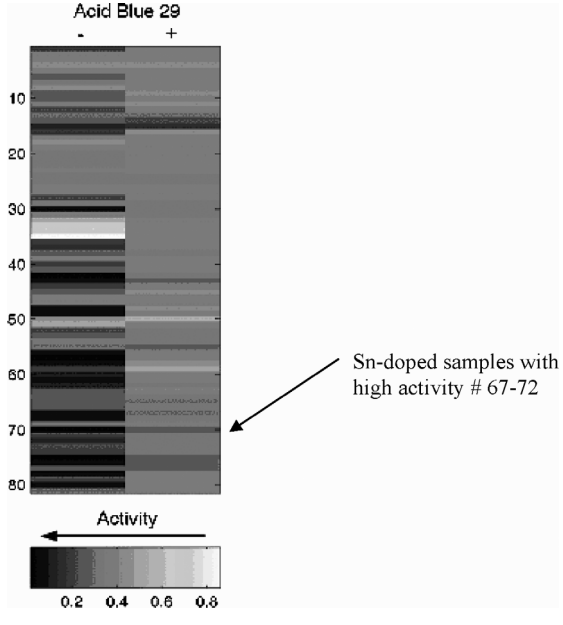

Figure 4. Result of the high-throughput screening experiments during degradation of Acid Blue 29: depicted are two bands of colour coded stripes representing the DOP values for the 81 different samples (top–down, see Tables 1–4 for the different dopants) for the activity of the respective catalysts for 5 min full spectrum irradiation (left column, $-$) or 20 min irradiation through a 400 nm cut-off filter (right column, $+$). Lower DOP values represent higher activity and are shown in darker colours.

Based on this data it is difficult to decide which ones are the best catalyst samples. Thus, in order to compare the average performance of the catalysts, a ranking has to be made. As the DOP for the individual dyes values cover different ranges, the data has to be normalized, i.e., divided by the maximum DOP on the individual dye. Based on these normalized data, the catalysts were sorted in increasing order by their mean DOP (averaged over the dyes). As the DOP and the activity are inversely related, this yields a decreasing ranking of the catalyst performance such that position 1 represents the catalyst with the best average performance. The results for the averaged activity rankings are shown in Table 5 for the full spectrum illumination and in Table 6 for the visible spectrum only irradiation.

As it clearly could be seen in Figs 2–4 and in Tables 5 and 6 the systems doped with tin (samples 67–72) show the highest activities and, in addition to this, it also could be clearly seen that there is a big difference between the results obtained by the full light irradiation compared to the irradiation through the cut-off filter.

Table 5.
5 min full emission spectrum illumination activity ranking with normalized data

Rank	Catalyst no.	Averaged activity
1	49	0.052
2	70	0.102
3	68	0.138
4	67	0.140
5	48	0.142
6	78	0.153
7	71	0.162
8	30	0.166
9	42	0.168
10	16	0.173
29	1 (reference)	0.245

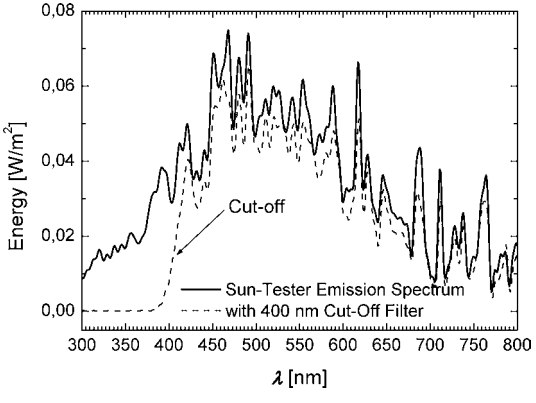

Figure 5. Emission spectra of the sun tester (Atlas-Suntest CPS+, 750 W/m^2 Xenon lamp) used for illumination of photocatalyst/dye mixtures.

Table 6.
20 min 400 nm cut-off filter restricted illumination activity ranking with normalized data

Rank	Catalyst no.	Averaged activity
1	70	0.236
2	65	0.287
3	67	0.300
4	68	0.311
5	71	0.333
6	55	0.336
7	38	0.345
8	66	0.348
9	32	0.353
10	64	0.362
42	1 (reference)	0.492

As shown in Table 3, these systems represent the following compositions and treatments. In these samples variations of the $Ti(OiPr)_4$ (samples 69, 71 and 72) concentrations were tested. Numbers 69 and 71 had 35 wt% $Ti(OiPr)_4$ in the reaction mixture and sample 72 had 20 wt%, respectively. Numbers 67, 68 and 70 were treated at 250°C for 120 min. Finally the concentration of dopant was varied from 0.5 mol% (samples 67) over 1 mol% (samples 68, 69) and 2.5 mol% (samples 70) to 5 mol% (samples 71, 72).

As it can be seen not all possible permutations have been tested yet: given the excellent activity, further variations are planned.

From the screened particle lots three of them (samples 70, 57 and 65) were selected for further testing applying the stearic acid procedure. The selected particles for these stearic acid degradation experiments based on the ranking were sample 70 (2.5 mol% $SnCl_4$, treated at 250°C for 120 min), which had the best overall ranking, a species with a very low activity, sample 57 (doped with 1 mol% $Nd(OMeOEt)_3$, treated at 225°C for 90 min) and an undoped material was also selected (sample 65, 35% Ti $(OiPr)_4$, treated at 250°C for 60 min), because this material showed good day light activity (rank 2).

Stearic acid decomposition tests

In order to find out how far the results obtained with the dye decomposition tests show significance for practical application a different model system was selected for further experimental work. The degradation of stearic acid layers on photocatalytically-active surfaces was selected due to the resemblance to real world degradation of fatty stains on surfaces. This degradation can easily be followed by measuring the contact angle of the surface against water. The experimental effort to prepare the surface modification of the particles, the coating sols and the coating process is so huge that testing of all prepared particle batches prohibits itself. Thus, a suitable selection of promising candidates for the further testing has to be done.

The ranking which was obtained by the high-throughput screening process gave a suitable tool. Nevertheless, not only very active particles but also an ineffective (compared to the base, i.e., undoped titania) were selected for comparison purposes.

The selected powders were surface modified and coated on glass substrates as gradient two-layer systems as described in Section 2. These two-layer systems consist of a barrier layer, based on the described binder-system, with a surface layer of active photocatalyst material.

For comparison a single-layer coating system as developed in INM has also been tested. This system is a self-organising gradient system with a different preparation method. Fluoroorganically-modified titania nano-particles are introduced as a methyl ethyl ketone sol into a binder-system. During the curing due to the different rates of evaporation of the solvents, a decompatibilisation between the coated particles and the matrix material occurs, which leads to a diffusion of the particles to the interface between coating and air [16, 17]. The results of this mechanism are shown in a TEM microphotograph (Fig. 6). In Fig. 6 one can easily recognise the titania particles which have been enriched at the interface between the coating and the air. After complete curing, the material is activated by UV-irradiation and shows good self-cleaning and superhydrophilic properties [15].

In order to check for further effects such as photolysis or evaporation photocatalytically inactive glass plates were also examined.

For the degradation experiments the five types of substrates were dip-coated with stearic acid In this case the surface concentration of the stearic acid was $126 \pm 3.5\ \mu g/cm^2$ and the contact angles of the coated substrates was in the range of 70 to 80°.

The results of the degradation experiments are depicted in Figs 7 and 8 for the different irradiation sources, respectively. In Figs 9 and 10, respectively, the spectra of the two light sources applied are shown in comparison to the solar irradiation measured in Saarbrücken by the end of March at noon under clear sunny skies. Figure 9 depicts the photon flux as a function of the wavelength, whereas in Fig. 10 the energy per wavelength is shown.

These results can be interpreted in the following ways.

First, it can be seen that neither of the light sources is significantly reducing the contact angle on the inactive glass plate which was used as a reference during the time scale of the respective degradation experiment. Thus, it can be presumed that the photocatalytic effect of the active surfaces is responsible for the observed reduction in the contact angle.

Second, it can be seen that the double-layer systems show higher degradation activities than the single-layer system. This can be attributed to the higher surface concentration of active material which can be deposited by the second coating step compared to the small amount of active material which can be incorporated in the single layer lacquer material. This can also be seen in the TEM microphotograph (Fig. 6). The thickness of this active layer is rather small, only a few tens of nanometers, which is the cause for the low photocatalytic degradation activity.

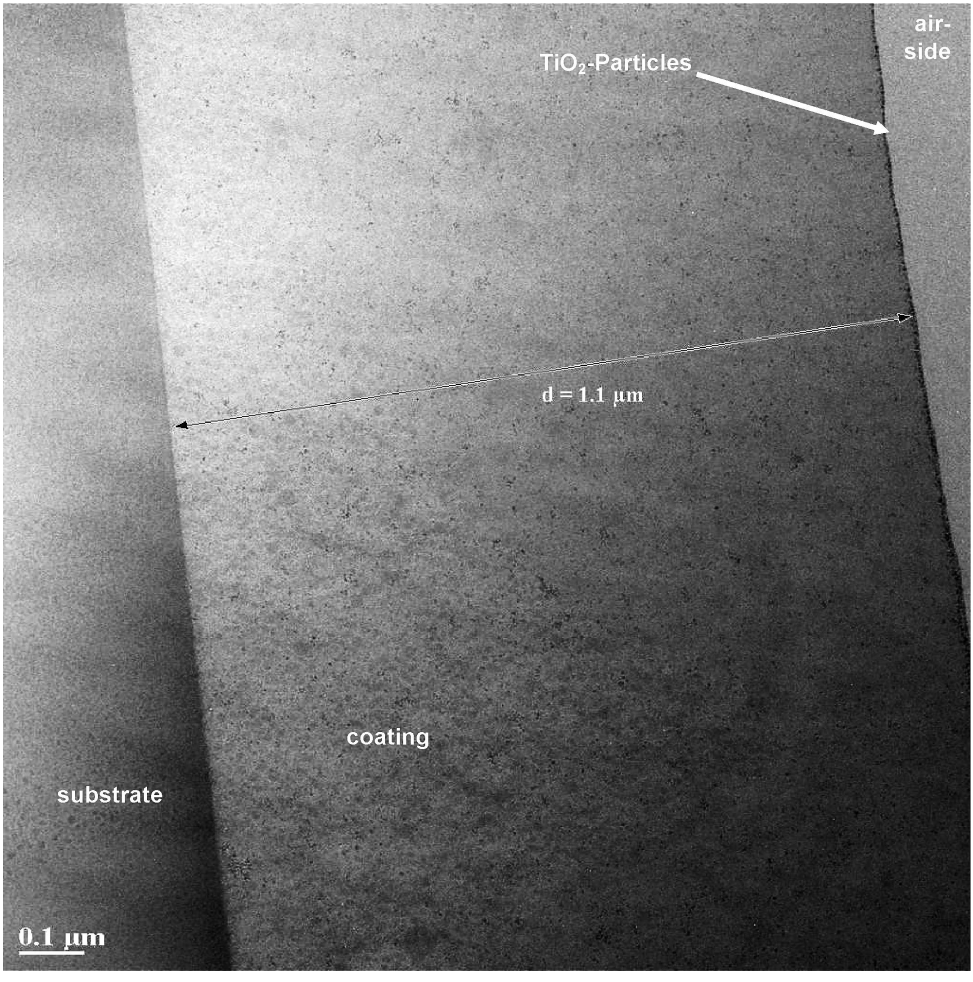

Figure 6. TEM microphotograph of a single layer system. From left to right: substrate — coating (thickness 1.1 μm) — air side. The titania particles are enriched at the interface between coating and air side and can be seen as small black dots.

Nevertheless, the single-layer material shows a sufficient superhydrophilicity and self-cleaning capability in real applications. In the plots STFull and ST400-800 the same light source has been used; for the ST400-800 only the addition of a 400 nm edge filter has cut off all wave lengths below 400 nm. From a comparison of the spectra, it now can be calculated that these photons below 400 nm attribute for a total of only 9.98% of the total photon number of STFull. But when taking into account the energy of the photons, it can be seen that 48.8% less energy is irradiated under the conditions of ST400-800. The lower photon flux and thereby lower energy flux are responsible for the difference in degradation efficiency.

It can be stated that the remaining photons do not have enough energy to significantly induce photocatalytic activity in the Nd-doped titania (sample 57).

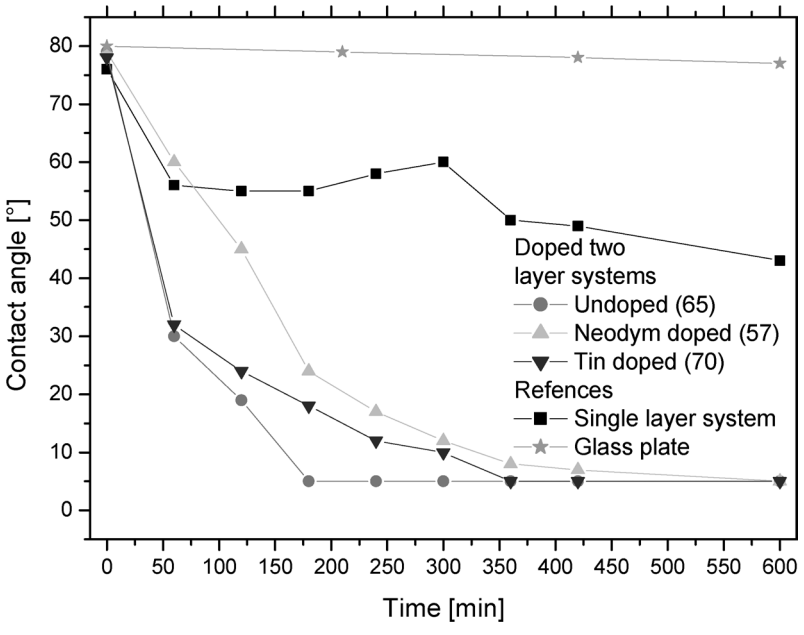

Figure 7. Stearic acid degradation experiment applying the Suntester STFull source.

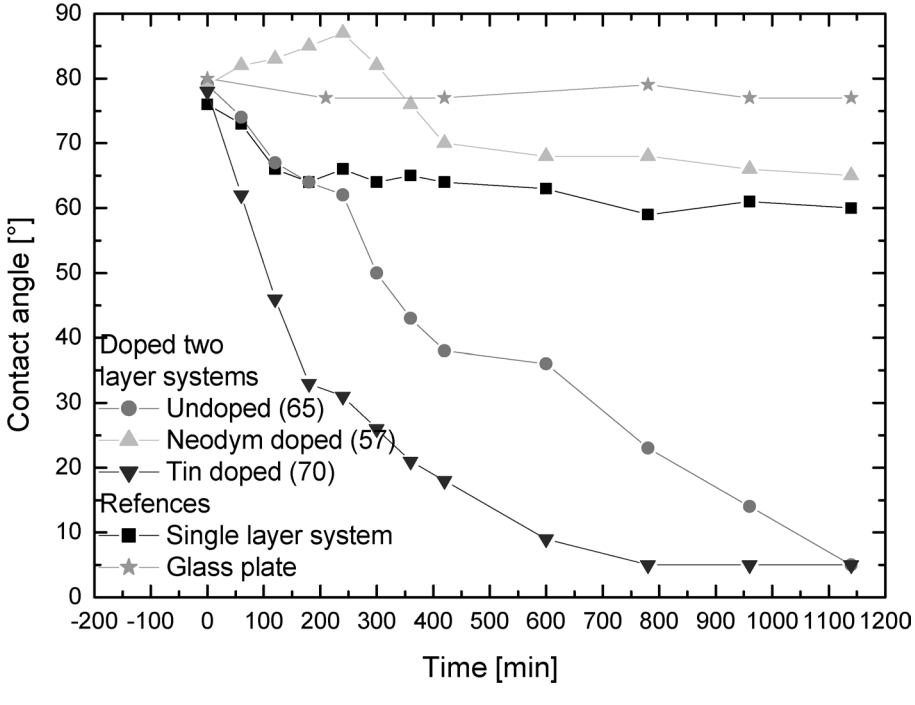

Figure 8. Stearic acid degradation experiment applying the Suntester ST400-800 source.

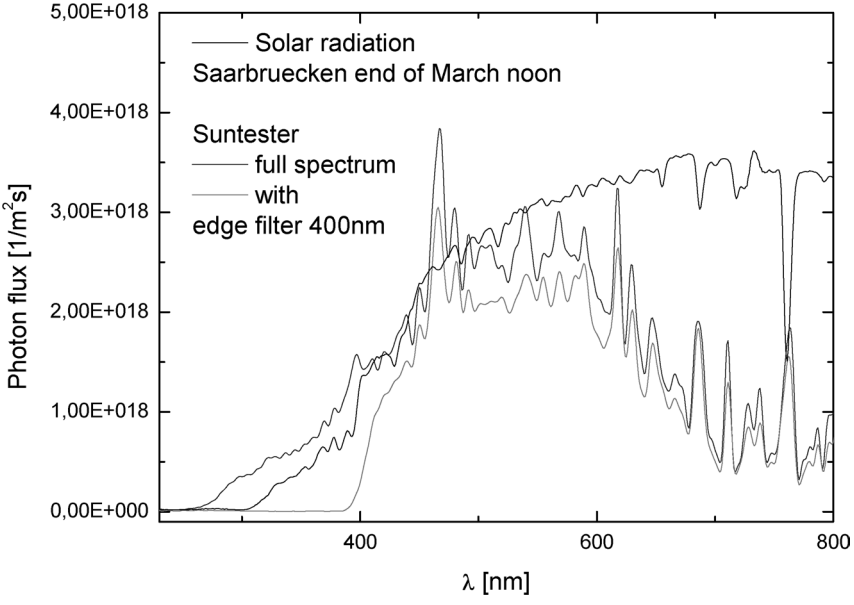

Figure 9. Photon flux spectra of the utilized suntester with and without the edge filter 400 nm in comparison to a solar spectrum.

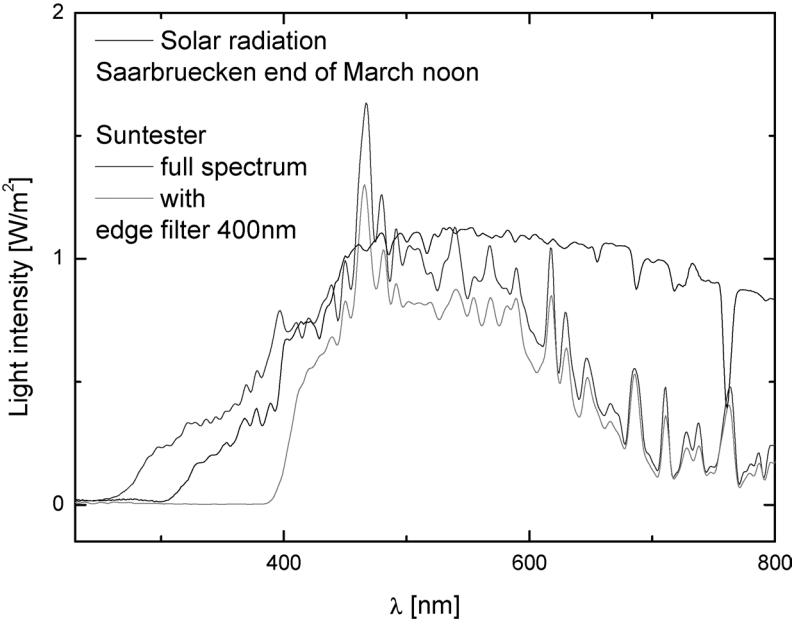

Figure 10. Energy spectra of the utilized suntester with and without the edge filter 400 nm in comparison to a solar spectrum.

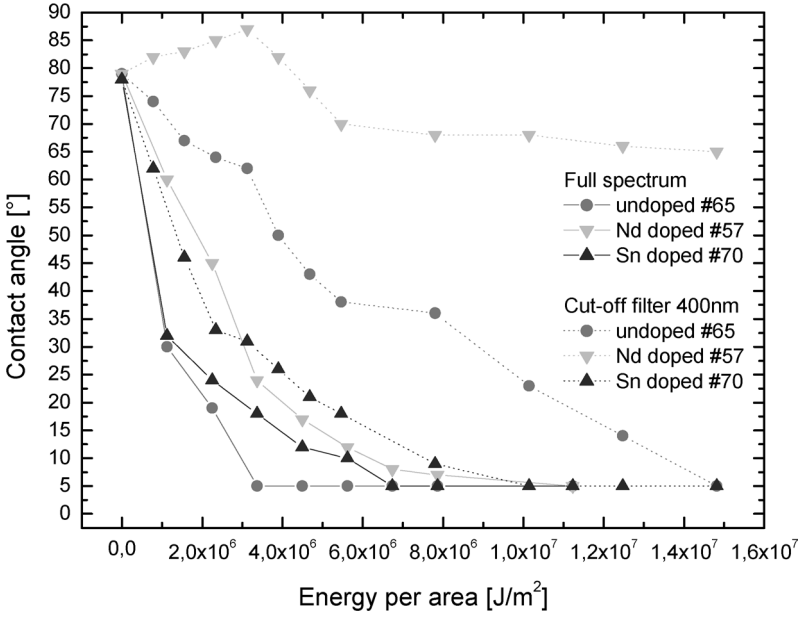

Figure 11. Decrease of the contact angle in the different degradations experiments as a function of the total energy.

Secondly, for the Sn-doped (sample 70) and the undoped material (sample 65) the daylight activity can be estimated based on the time needed for a total removal of the stearic acid. This can be approximated by the time when a contact angle of 5° or lower is resumed by the surface.

Under the conditions of STFull this happens after about 180 min for the undoped material (sample 65) and after 360 min for the Sn-doped material (sample 70), respectively. For the visible light only irradiation under the ST400-800 regime the contact angle reaches 5° after 780 min for the Sn-doped system and after 1140 min for the undoped system. For the irradiation with visible light only the Sn-doped material is slower by only a factor of 2.17. The undoped material on the other hand needs 6.4-times longer when only visible light is present for the same reaction. Thus, it can easily be seen that the Sn-doped material exhibits a significantly higher daylight activity than the undoped material. Furthermore, we can interpret the different responses to the various light sources. For this purpose we exchanged the time dependencies of the degradation experiments by the total photon number or the energy per area, respectively. These exchanges were made by multiplying the irradiation times of the two experiments with the number of photons per second and area or with the energy flux respectively. These data were calculated based on the spectra in Figs 9 and 10 and the results are shown in Figs 11 and 12. Figures 11 and 12 also confirm the above-mentioned visible light activity of the Sn-doped material. The degradation curve of the experiment applying the cut-off filter is slightly tailing the experiment executed with the full spectrum. The general

shape of the degradation is the same. For the other materials it can be seen that even after normalizing the reaction time towards total energy or total photon number, the tailing is much greater. The general form of the degradation curves is also changing from an exponential to a linear decrease.

Another important conclusion can be made based on the presented results especially with respect to the spectra presented in Figs 9 and 10. The spectrum of the sun tester is in good approximation comparable to the solar spectrum up to about 500 nm. Furthermore, the spectrum resembles that of the sun tester with the cut-off filter applied a spectrum of solar light through a window pane. Thus, the data obtained by such degradation experiments can be extrapolated to real world degradation on photocatalytic surfaces. It has to be borne in mind, however, that the energies are only comparable at noon. Thus, degradations times of 12 or 19 h, as found in our experiments, would last several days at least using solar light indoors.

The presented results for the degradation experiments and their interpretation are only an approximation of the real visible light photocatalytic activity, depending on the differences in activation by the blue and green parts of the spectrum. These can be used to make a rough estimation of the daylight activity of newly developed photocatalyst materials. It has to be further examined which changes and improvements to the method described here have to be made to give it a greater significance.

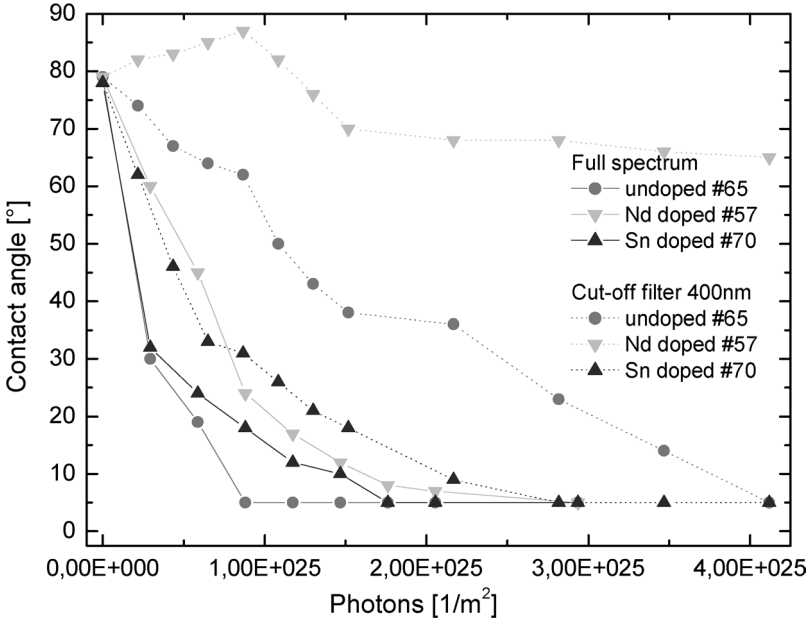

Figure 12. Decrease of the contact angle in the different degradations experiments as a function of the total number of photons.

CONCLUSIONS

It can be said that the method described here for a fast screening of a large number of different catalyst samples followed by testing of selected samples under more realistic conditions can lead to a vast reduction of the development time for new photocatalytic materials. Thus, a lot of work wasted on ineffective catalysts can be saved by an intelligent selection of the most promising materials by the presented method. Of course there are many questions open. No investigations about the mechanisms have been carried out so far. In the next steps, the microstructure of the highly active photocatalysts will be investigated and optimized, and coatings for various applications will be developed. The first investigations using the presented high-throughput method are promising for a fast selection of the most active species.

Acknowledgements

The author wants to thank the Government of the Federal Republic of Germany, the State of Saarland and various industrial companies for their financial support, and Dr. Th. Krajewski and R. Karos for their experimental help and their fruitful discussions.

REFERENCES

1. K. Honda and A. Fujishima, *Nature* **238**, 37 (1972).
2. A. Fujishima, K. Hashimoto and T. Watanabe, *TiO_2 Photocatalysis: Fundamentals and Applications*. BKC, Tokyo (1999).
3. A. Nakajima, M. Miwa, K. Abe, K. Hashimoto and T. Watanabe, in: *Proceedings of the 3rd ICCG*, p. 253. Universal Press, Veenendaal (2000).
4. M. Hayakawa, T. Watanabe, K. Norimoto, E. Kojima, M. Machida, Y. Saeki, T. Kuga and Y. Nakajima, Japanese Patent No. 2002119865 A (2002).
5. T. Watanabe, M. Hayakawa, M. Chikuni and A. Kitamura, Japanese Patent No. 20012443820 A (2001).
6. M. Hayakawa, T. Watanabe, K. Norimoto, E. Kojima, M. Machida, Y. Saeki, T. Kuga and Y. Nakajima, Japanese Patent No. 2001200627 A (2001).
7. J. M. Herrmann, A. Assabane, A. I. Yahia, H. Tahiri and C. Guillard, *Appl. Catal. B* **24**, 71 (2000).
8. H. Kisch and W. Lindner, *Chem. Unserer Z.* **35**, 250 (2001).
9. L. Zang, W. Macyk, Ch. Lange, W. F. Maier, Ch. Antonius, D. Meissner and H. Kisch, *Chem. Eur. J.* **6**, 379 (2000).
10. W. Macyk and H. Kisch, *J. Inf. Rec.* **25**, 435 (2000).
11. S. Sakthivel and H. Kisch, *Angew. Chem.* **115**, 5057 (2003). Accessible online at http://dx.doi.org/10.1002/ange.200351577
12. K. Morikawa, Y. Taga, T. Nakamura and Y. Fukushima, Japanese Patent No. 2002095916 (2002).
13. J. Yang, D. Li, X. Wang and L. Lu, *J. Solid State Chem.* **165**, 193 (2002).
14. M. Akarsu, E. Arpac and H. Schmidt, WO Patent No. 2004/005577.
15. H. Schmidt, M. Akarsu, M. Naumann and Th. S. Müller, Doped nanoparticles for photocatalytically active surfaces (in press).
16. H. Schmidt, *Glastechn. Ber. Glass Sci. Technol.* **68**, 21 (1995).
17. R. Kasemann and H. Schmidt, *New J. Chem*. **18**, 1117 (1994).